Quantification of CO2 uptake of concretes with mineral additions after 10-year natural carbonation

Akli Younsi, Philippe Turcry, Abdelkarim Aït-Mokhtar

Quantification of CO_2 uptake of concretes with mineral additions after 10-year natural carbonation

Akli Younsi, Philippe Turcry*, Abdelkarim Aït-Mokhtar

La Rochelle University, LaSIE UMR CNRS 7356, Avenue Michel Crépeau, 17042 La Rochelle Cedex 1, France

* Corresponding author.

E-mail address: philippe.turcry@univ-lr.fr (Ph. Turcry),

Postal address: La Rochelle University, LaSIE UMR CNRS 7356, Avenue Michel Crépeau, 17042 La Rochelle Cedex 1, France

E-mail addresses: akli.younsi@univ-lr.fr (A. Younsi), philippe.turcry@univ-lr.fr (Ph. Turcry), karim.ait-mokhtar@univ-lr.fr (A. Aït-Mokhtar)

ABSTRACT

The CO_2 uptake of Portland cement, fly ash and blast furnace slag concrete cylinders was determined after 10-year natural carbonation. The purpose was to provide data to better assess the exchanges of CO_2 during the life cycle of structures. The CO_2 uptake of cylinders (mass of bound CO_2 per unit of surface) was calculated from profiles of CO_2 content determined by thermogravimetric and chemical analyses. The CO_2 binding capacity of concrete with high slag content was found much lower than that of Portland cement concrete, due to the low

degree of carbonation of CaO from slag. The CO_2 uptakes of the studied specimens were however rather close. High carbonation depth of slag concretes compensates partly their lower binding capacity. The experimental results were compared to predictions of the European Standard EN 16757 model. The Standard model underestimates the CO_2 uptake of concretes with mineral addition mainly because of an underestimation of the carbonation depth.

Keywords:

CO_2 uptake

Blended cement

Fly ash

Ground granulated blast-furnace slag

Natural carbonation

Sheltered/unsheltered natural exposure

Bound CO_2 content

Degree of carbonation

European Standard EN 16757

Wordcount : 10623 words

1. Introduction

Life cycle analyzes showed that cement production, responsible for 65 – 85 % of CO_2 emissions from concrete manufacturing, accounts for 5 – 8 % of global CO_2 emissions (Miller et al., 2016; Olivier et al., 2016; Andrew, 2019; Lim et al., 2019). Therefore, efforts to mitigate CO_2 emissions from concrete manufacturing have focused on: (i) using alternative fuels and raw materials during cement production, (ii) developing alternative low-carbon binders, (iii) substituting with raw or mineral materials a part of clinker during cement production or a part of cement during concrete manufacturing (Flower et al., 2007; Younsi et al., 2013; Gartner et al., 2015; Feiz et al., 2015; Elchalakani et al., 2017; Younsi et al., 2019; Costa et al., 2020; Ren et al., 2020; Esfahani et al., 2021; Younsi et al., 2021). However, to establish a more complete life cycle inventory of concrete in terms of carbon footprint, in addition to accounting for the CO_2 emissions due to its manufacture, it becomes essential to consider also the CO_2 uptake due to its carbonation (Lagerblad et al., 2005; Galan et al., 2010; Ashraf, 2016 ; Jang et al., 2016 ; Lee et al., 2016 ; Possan et al., 2016 ; Andrade et al., 2018; Andersson et al., 2019; Sanjuán et al., 2019; Sanjuán et al., 2020; Witkowski et al., 2020; Kwon et al., 2021). The CO_2 uptake is defined as the quantity of CO_2 bound by a concrete structure and expressed in mass of bound CO_2 per unit area of this structure. For instance, the study conducted by Pade and Guimaraes showed that, after 70 years, concrete structures produced in 2003 will bind about 28 % of the CO_2 emissions from cement production (Pade et al., 2007). (Yang et al., 2014) showed that concrete structure will bind 18 – 21 % of the CO_2 emissions from cement production, after 100 years. (Fitzpatrick et al., 2015) showed that structures built in 1972 will bind, after 100 years, about 16 % of the CO_2 emissions from cement production. The study of (Xi et al., 2016) showed that, due to their natural carbonation

occurring between 1930 and 2013, cementitious materials have bound 43 % of the CO_2 emissions from cement production for the same period. The authors concluded that carbonation is an important carbon sink which is not yet included in life cycle inventories.

Carbonation is a natural aging process during which atmospheric CO_2 diffuses into the pore network of concrete and chemically reacts with hydration products, forming mainly $CaCO_3$ (Papadakis et al., 1991). This phenomenon can be considered from two opposing points of view depending on how the role of chemical reactions involving CO_2 is considered: (i) from the point of view of durability of reinforced concrete structures, chemical reactions between CO_2 and hydration products can initiate the rebar corrosion by lowering the *pH* of the pore solution. Carbonation is thus considered as a degradation phenomenon expected to reduce the service life of structures, (ii) from the point of view of environmental impact, the chemical reactions involving CO_2 allow bounding CO_2 within the concrete. Carbonation is thus considered as a process contributing to the reduction of CO_2 emissions from concrete manufacturing and use.

As pointed out by Andrade, very few studies were devoted to the quantification of bound CO_2 (Andrade, 2020). The calculation of CO_2 uptake remains a very complex task since only approximate calculation methods and empirical models are used (Andersson et al., 2013). A standardized calculation method is presented in the Annex BB of the European Standard EN 16757 (EN16757, 2017). The standard allows assessing the CO_2 uptake at different life cycle stages by assuming a direct link between carbonation and amount of reactive CaO in concrete. To assess the CO_2 uptake occurring during a given period, EN 16757 refers to the concepts of: (i) carbonation rate, which is defined by considering both the compressive strength class and the exposure conditions, (ii) degree of carbonation (ratio between carbonated and available reactive CaO), (iii) maximum theoretical uptake of CO_2 in totally carbonated concrete which is correlated with the reactive CaO content in the binder. Results

from some published works, such as those carried out by (Yang et al., 2014) and (Fitzpatrick et al., 2015), are consistent with the calculations from EN 16757 in terms of CO_2 uptake. However, the findings provided by these studies remain theoretical long-term assessments (up to 100 years) that are difficult to validate with experimental data due to the lack of availability of the latter, as mentioned previously (Andrade, 2020). It thus appears interesting to compare experimental results obtained over a realistic and sufficiently long period exposure to natural carbonation with prediction of models such as the EN 16757 standard model. Moreover, there is also a lack of data on the CO_2 uptake of concrete made with blended binders that are increasingly used to the detriment of Ordinary Portland Cement (OPC) to reduce the footprint of concrete use.

In the view of these considerations, the present work aims at providing data on CO_2 uptake due to atmospheric carbonation of various concretes. There is still a lack of this type of data in the literature, especially for concretes with mineral additions. These data are necessary to better assess the real environmental footprint of the use of concrete in civil engineering structures with approach such as the one proposed by (Xi et al., 2016).

For this purpose, an experimental study was carried out on concretes designed with OPC, blended cements containing fly ash or ground granulated bast furnace slag (GGBFS), and partial substitutions of OPC with fly ash or GGBFS. The concretes were subjected to 10-year natural carbonation, under sheltered and unsheltered conditions. During the exposure period, the progress of carbonation was monitored by regular carbonation depth measurements. At the end of the exposure period, the CO_2 uptake was determined by Thermogravimetric analysis (TGA) coupled to chemical analysis by Inductively Coupled Plasma - Atomic Emission Spectroscopy (ICP-AES). In the following, the results of this experimental investigation are analyzed to assess the effect of both binder nature and exposure on CO_2 binding capacity, degree of carbonation and CO_2 uptake of the studied specimens. Finally, the experimental

results are compared to calculations using the EN 16757 model and its range of validity is discussed.

2. Materials and methods

2.1. Materials

The study was carried out on concrete mixtures designed with three cements as per the European Standard EN 197-1 (EN197-1, 2011): an Ordinary Portland Cement CEM I 52.5 N ~~from Lafarge France~~, a blended cement CEM II/B-V 32.5 R ~~from CCB Belgium~~, and a ground granulated blast-furnace slag cement CEM III/C 32.5 N ~~from Calcia France~~. Other constituents were used: a fly ash (FA) with low calcium content ~~from Surschiste France~~ as per the European Standard EN 450-1 (EN15167, 2006), a ground granulated blast-furnace slag (GGBFS) ~~from Ecocem Netherlands~~ as per the European Standard EN 15167-1 (EN15167, 2006), a siliceous sand (0/4 mm) and two crushed diorite gravels (6.3/10 and 10/14 mm) ~~from HeidelbergCement France~~ as per the European Standard EN 13139 (EN13139, 2003), and a polycarboxylate superplasticizer ~~Fluid Optima 206® from Chryso France~~ as per the European Standard EN 934-2+A (EN934-2, 2012). Table 1 shows the properties of the cementitious materials used. The chemical compositions of the binders were obtained by X-ray fluorescence (XRF) analysis. Note that the used sand is a sea sand which contains trace of limestone due to shell particles. Its mass content of $CaCO_3$ is equal to 6.9%.

Table 1

Physical, mineralogical, and chemical properties of the cementitious materials used.

Cements			Mineral additions	
CEM I	CEM II	CEM III	FA	GGBFS

Physical properties					
Density [kg/m^3]	3110	2890	2900	2210	2890
Blaine surface [cm²/g]	3400	3247	4280	4050	4500
Composition [w%]					
Clinker	95	73	15	0	0
Gypsum	5	4	3	0	0
Fly ash	0	23	0	100	0
GGBFS	0	0	82	0	100
Limestone	0	4	3	0	0
Chemical composition [w%]					
CaO	64.8	48.9	45.1	5.2	41.5
SiO_2	20.5	27.4	32.0	55.3	33.3
Al_2O_3	4.5	9.0	10.3	25.2	12.5
Fe_2O_3	2.7	3.4	0.8	6.4	0.4
SO_3	3.5	2.8	2.9	0.5	0.2
MgO	1.5	2.0	6.1	0.9	7.0
Clinker mineralogical composition [w%]					
C_3S	67	69	66	-	-
C_2S	13	10	13	-	-
C_3A	7	9	11	-	-
C_4AF	8	7	7	-	-

2.2. Mixtures

The proportions used in the mixes are given in Table 2. Three concrete mixtures were used as references: Ref I with CEM I, Ref II with CEM II and Ref III with CEM III. Three other concrete mixtures were designed with partial substitution of CEM I with FA (FA 30) or GGBFS (S 30 and S 75). Except for S 75, all the mixtures were designed as per the prescriptive requirements from the French annex of the European Standard NF EN 206/CN (EN206/CN, 2014) corresponding to the exposure class XC 3. These requirements are the following: a minimum strength class C25/30, a minimum equivalent binder content (Eq.binder) of 280 kg/m^3, a maximum effective water-to-equivalent binder ratio (W/Eq.binder) of 0.6, and a maximum cement substitution ratio (A/(A+C)) of 30 % for FA 30 and S 30. It should be noted that the requirements corresponding to XC 3 are equivalent to

1 those corresponding to XC 4. Moreover, the mixture S 75, which does not comply with the
2 prescriptive requirements of EN 206, was designed with a cement substitution ratio of 75 %
3 using the mix-design method suggested by (Khokhar et al., 2010). Its effective water-to-
4 binder ratio (W/(A+C)) was optimized using the Bolomey's equation to obtain a 2-day
5 compressive strength of 10 MPa. Finally, for all the mixtures, the amount of superplasticizer
6 was adjusted to obtain a slump higher than 150 mm. Additional details on the mix-design
7 method used can be found in (Younsi et al., 2011). In summary, the six studied concretes are
8 equivalent in terms of site construction application, since they have the same workability and
9 mechanical performances at early age and 28 days.

10 The concrete mixtures were cast, according to the European Standard EN 12390-12
11 (EN12390-12, 2020), into Ø11X22 cm molds and stored in a room at 20 ± 1 °C for 24 h.
12 Other physical, chemical and mechanical properties are given in Table 2. Especially, Table 2
13 gives the total mass of CaO from the $CaCO_3$ of both sand and binder and from the anhydrous
14 elements of binder (e.g., C_3S, C_2S). The parameter denoted α is the fraction of CaO from the
15 binder to the total mass of CaO.

16

17 **Table 2**

18 Mix proportions per cubic meter of concrete and properties.

	Ref I	Ref II	Ref III	FA 30	S 30	S 75
CEM I 52.5 N [kg]	303	0	0	241	219	103
CEM II/B-V 32.5 R [kg]	0	321	0	0	0	0
CEM III/C 32.5 N [kg]	0	0	361	0	0	0
Fly ash [kg]	0	0	0	103	0	0
GGBFS [kg]	0	0	0	0	94	310
Gravel 10/14 [kg]	875	875	859	844	868	836
Gravel 6/10 [kg]	211	211	207	204	209	201
Sand 0/4 [kg]	855	855	839	824	848	816
Effective water [kg]	182	175	175	182	182	170
Superplasticizer [kg]	1.36	1.00	1.00	1.75	0.26	1.89
W/(A+C) [-]	0.60	0.54	0.48	0.53	0.58	0.41
Binder content [%]	12.5	13.2	14.8	14.4	12.9	16.9

Eq.binder [kg]	303	321	361	303	304	223
W/Eq.binder [-]	0.60	0.54	0.48	0.60	0.59	0.76
Clinker [kg]	288	234	54	229	208	98
Total CaO from binder and sand [kg]	229	190	195	193	214	227
CaO from binder [kg]	196	157	163	161	181	195
α [-]	0.86	0.83	0.83	0.83	0.85	0.86
28-day water porosity [%]	13.8	12.6	16.7	14.4	13.5	13.7
28-day compressive strength [MPa]	36	32	34	33	36	40

A = Mineral addition; C = Cement; W = Effective water; Eq.binder = Equivalent binder

2.3. Carbonation conditions

Immediately after demolding at 1 day, the Ø11X22 cm specimens were subjected to natural carbonation under sheltered conditions (exposure class XC 3 as per EN 206) and unsheltered (XC 4) conditions for 10 years. This demolding at early age is not favorable for some concretes, such as GGBFS concrete (Ref III), but this makes the study conditions more representative of in working site conditions (i.e., poorly hydrated concrete cover), which interest the project managers. Table 3 gives the ranges of temperature and relative humidity at both exposure sites located in La Rochelle, France. In unsheltered conditions, the specimens were placed on the floor of an outside laboratory platform. So, they were subject to rain, wind, and solar radiation. Over the 10 years, the specimens were sometimes rotated, so that the effect of solar radiation is on all sides. In the sheltered conditions, the specimens were placed on shelves protected from external climatic conditions (rain and sun).

Table 3

Temperature and relative humidity at both exposure sites: averages and ranges (minimum and maximum were obtained from 2-day moving averaging).

	Sheltered conditions	Unsheltered conditions
Temperature (°C)	18 (14 – 26)	13 (2 - 26)
Relative humidity (%)	70 (30 – 80)	77 (50 – 95)

2.4. Determination of carbonation depths by phenolphthalein spraying

Carbonation depths were determined at 1, 2, 3, 6 and 10 years on Ø11X5 cm specimens saw-cut from the Ø11X22 cm specimens. The Ø11X5 cm specimens were split in half and a *pH* indicator solution, namely a solution of 1% phenolphthalein, was sprayed on the split sections to assess the carbonation depth as per the European Standard EN 12390-12 (EN12390-12, 2020). Before spraying phenolphthalein, the top and the bottom of the Ø11X22 cm specimens were removed to only consider the carbonation depths due to radial CO_2 diffusion. The carbonation depth is the mean value of depths d_i determined as shown in Fig. 1. It should be kept in mind that phenolphthalein reveals area where pH is lower than 9 and not strictly speaking a fully carbonated area.

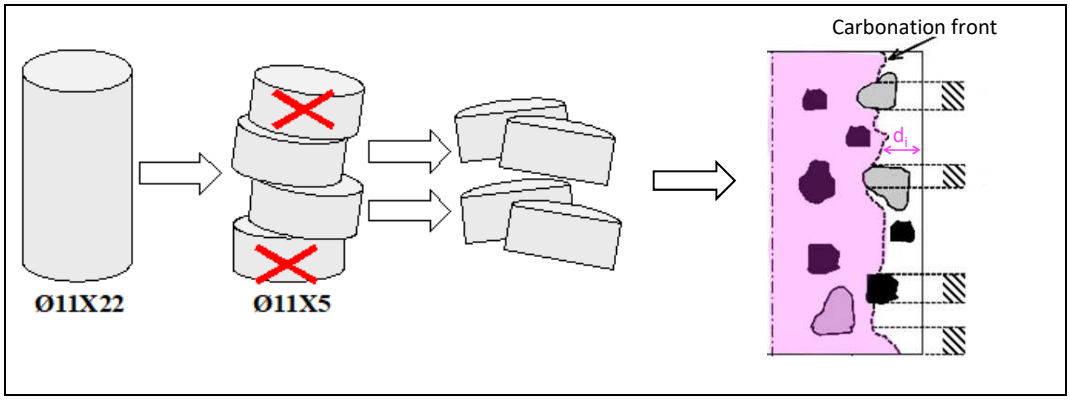

Fig. 1. Schematic presentation of the carbonation characterization by phenolphthalein spraying: sawing of cylindrical specimen, then splitting of the obtained discs, and finally determination of carbonation depths (d_i) after phenolphthalein spraying. Depths d_i are measured outside the hatched zones (EN12390-12, 2020).

2.5. Carbonation characterization by TGA coupled to chemical analysis ICP-AES

Carbonation measurements were carried out after 10-year exposure by determining the bound CO_2 contents in concrete powders. The latter were obtained by drilling holes in Ø11X5 cm specimens, themselves saw-cut from the Ø11X22 cm specimens (Fig. 2). Before drilling holes, the top and the bottom of the Ø11X22 cm specimens were removed to only consider the radial carbonation. The centers of the holes were located at 4 different distances, from the core, chosen according to the carbonation depths revealed by phenolphthalein: 0; 15 – 20; 20 – 35 and 35 – 45 mm. For a given Ø11X5 cm specimen, a Ø8X50 mm hole was drilled through the core, and at each intermediate distance, 16 Ø5X50 mm holes were drilled. Moreover, the skin was removed to a depth of about 1 mm by planing. To avoid their carbonation, the powders were stored in a desiccator where the relative humidity was maintained at about 3 % by silica gel. The bound CO_2 contents were determined by thermogravimetric analysis (TGA) carried out on 210 ± 45 mg powders using a Setaram Setsys Evolution® device with a heating rate of 10 °C/min from 20 to 1000 °C in an argon atmosphere (Thiery et al., 2007; Bordy et al., 2017; Younsi et al., 2018). The mass of bound CO_2 corresponds to the loss of mass between 600°C and 900°C. In practice, this temperature range was refined by considering the derivative thermogravimetry (DTG) which reveals a peak at around 700°C due to the sample decarbonation. 2 to 3 replicates were used for TGA.

The bound CO_2 content determined by TGA is expressed in mg of CO_2 per mg of concrete powder. However, the powders are not enough homogenous and representative of the concrete. To express the bound CO_2 content as a function of a representative quantity of concrete, the binder content in each powder was assessed by chemical analysis (Turcry et al., 2014; Villain et al., 2007). The procedure consists of dissolving 100 ± 0.5 mg powder in 2 ± 0.01 mg nitric acid (HNO_3) for 24 hours. After that, a solution of HNO_3, with 1/50

dilution in pure water, is added. A week later, the suspension obtained is analyzed by Inductively Coupled Plasma-Atomic Optical Emission Spectroscopy (ICP-AES), using a Varian Vista device Pro®, to determine its CaO content. From the latter, it is possible to deduce the binder content in each concrete powder, as explained in section 3.2. One replicate for each sampling position was used for chemical analysis.

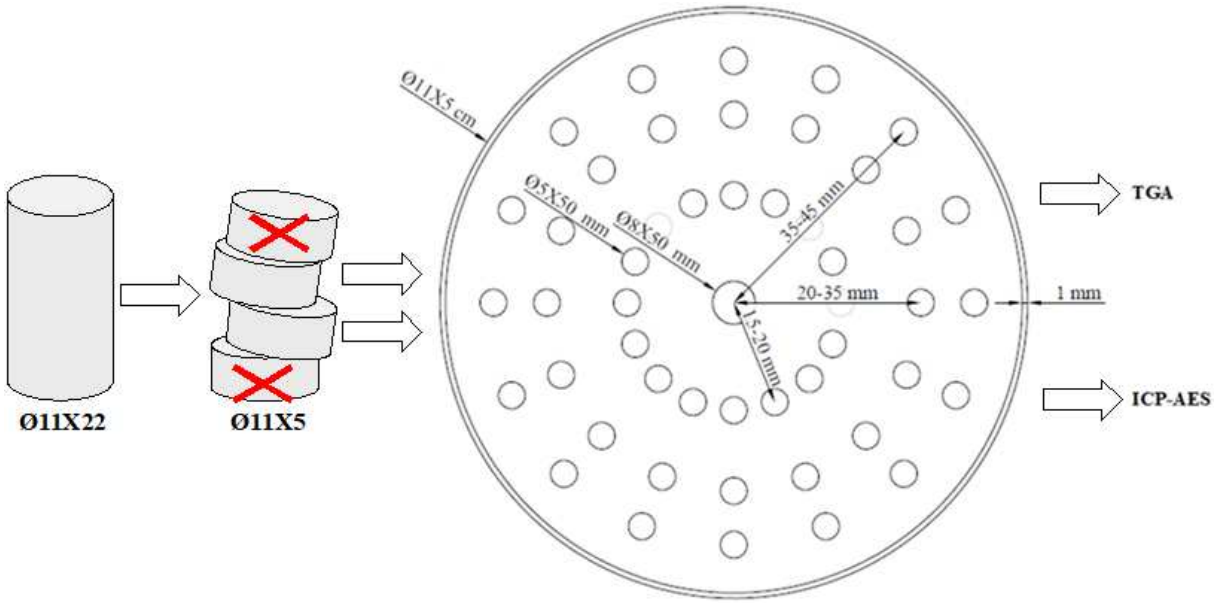

Fig. 2. Schematic presentation of the carbonation characterization by TGA/ICP-AES.

2.6. Calculation of CO_2 uptake from Standard EN 16575

An empirical model for the prediction of CO_2 uptake by cement-based products is proposed in the European Standard EN 16757. In the following sections, the predictions of this model are compared to our experimental results. To facilitate the comparison, we adopt the following nomenclature.

The uptake of CO_2 is expressed by exposure surface $[kg_{CO_2}/m^2]$ as follows:

$$\mathrm{Uptake(t)} = \mathrm{CBC}.\,\mathrm{X_c(t)} \quad (1)$$

Where: CBC is the CO_2 binding capacity of the carbonated zone [$\mathrm{kg_{CO_2}}$ per $\mathrm{m^3}$ of concrete] and $\mathrm{X_c(t)}$ is the carbonation depth [m] at an exposure time t [year].

In the model of European Standard, the carbonation depth is classically calculated as a function of the square root of time:

$$\mathrm{X_c(t)} = \mathrm{k}\sqrt{\mathrm{t}} \quad (2)$$

With: k the carbonation rate defined by considering the compressive strength class, the exposure conditions (sheltered or unsheltered), and the type and the dosage of mineral additions used.

The CO_2 binding capacity of the carbonated zone (CBC) is calculated with a conservative approach assuming that only the calcium oxides from clinker can be carbonated (Eq. 3). This approach is based on the point of view of the cement industry, since carbonation is seen in the scope of CCUS (Carbon Capture, Utilization and Storage) as a way to use or consume the CO_2 emitted during the production of clinker.

$$\mathrm{CBC} = \mathrm{K}.\,\mathrm{U_K}.\,\mathrm{DoC} \quad (3)$$

Where: CBC is the CO_2 binding capacity [$\mathrm{kg_{CO2}}$ per $\mathrm{m^3}$ of carbonated concrete], K the clinker content [$\mathrm{kg_K/m^3_{concrete}}$], $\mathrm{U_K}$ the maximum bound CO_2 by carbonation of CaO from the clinker [$\mathrm{kg_{CO2}/kg_K}$], and DoC the degree of carbonation [-]. The latter is defined as the ratio of the total bound CO_2 content for a given exposure and the theoretical maximum bound CO_2. Values of DoC are proposed for 3 exposures, i.e., indoor (0.40), outdoor sheltered (0.75),

outdoor unsheltered (0.85). U_K is usually taken equal to 0.5 kg_{CO2}/kg_K (for a CaO content in the clinker of around 65%).

To compare the model predictions with the experimental results, the model cannot be used as is, because the diffusion of CO_2 in our cylindrical specimens is radial. The square-root of time model given by Equation 2 is only valid for an axial diffusion. The calculated values of X_c must be corrected with the method presented in Appendix 1, which considers the cylindrical geometry for a sharp front carbonation. Knowing the corrected X_c, the CO_2 uptake is then calculated as follows:

$$\text{Uptake} = \frac{1}{R}\int_{Xc}^{R} CBC \cdot rdr = CBC\left[\frac{R^2 - (R - X_c)^2}{R}\right] \quad (4)$$

where: R [m] is the radius of the cylindrical specimen.

3. Results

3.1. Carbonation depths

Fig. 3 shows the time-evolution of the carbonation depths revealed after phenolphthalein spraying. For both sheltered and unsheltered conditions, FA 30 is more resistant against carbonation than Ref II, i.e. the reference with FA. S 30 and S 75 are more resistant than Ref III, i.e. the reference with GGBFS. In terms of natural carbonation, concretes with cement substitution thus exhibit a potential durability at least equivalent to that of the concretes with blended cements. By applying the concept of equivalent performance stated by the European Standard EN 206/CN, S 75, which does not comply with the prescriptive requirements of the standard, can replace at least Ref III. This result is consistent with previous studies on this

concrete mixture (Younsi et al., 2013; Younsi et al., 2019). Moreover, although Ref III complies with the prescriptive requirements of EN 206, it has the lowest resistance against carbonation. This is usually explained by the fact that, due to its very low clinker content, it has the lowest amount of carbonatable products ~~and the highest water porosity~~ (Table 2). Its CO_2 diffusion coefficient should be also the highest one because carbonation increases the CO_2 diffusivity of materials with high amount of GGBFS. For this kind of materials, recent papers give evidence of increase in gas diffusivity due to microstructural changes (Boumaaza et al., 2020a) or microcracking (Kangni-Foli et al., 2021) resulting from carbonation. ~~Ref I has the lowest carbonation rate, because it contains the highest clinker content, thus the highest amount of carbonatable products (Table 2). In addition, its CO_2 diffusivity should be the lowest since carbonation tends to decrease the gas diffusivity of materials with high amount of clinker (Boumaaza et al., 2020a).~~

Concretes exposed to carbonation under unsheltered conditions exhibit lower carbonation depths than those exposed to carbonation under sheltered conditions (relative deviations from 20 to 80 %). This result is expected because precipitation maintains the concrete pore network often close to saturation, what limits gas diffusion (Houst et al., 2002; Yoon et al., 2007; Ekolu, 2016 ; Huy Vu et al., 2019 ; Otieno et al., 2020). ~~The diffusion of CO_2 is thus only possible through the pore solution, which considerably slows down, the carbonation progress since CO_2 diffusion coefficient in air is known to be 10^4 times higher than that in water (Thiery, 2005). Carbonation occurs mainly when the pore network is sufficiently dry up to the carbonation depth reached before precipitation. Carbonation process is then mainly controlled by the frequency and duration of the wetting/drying periods.~~

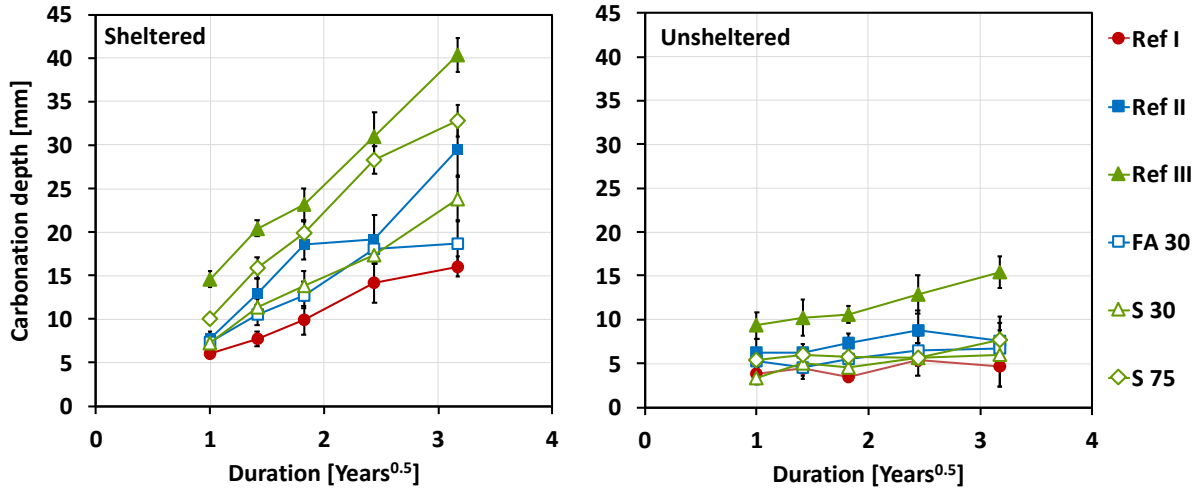

Fig. 3. Time-evolution of the carbonation depth in sheltered (left) and unsheltered conditions (right).

3.2. Binder content

Powder samples were obtained from drilling at different locations in the Ø11X5 cm specimens. Chemical analyzes allowed assessing the CaO content (%CaO) in these powder samples. The CaO is obtained from both the binder and the marine sand (the CaO comes from shells contains in the sand). Let us assume that the mass fraction α, as defined in section 2.2 and given in Table 2, is the same for the powder sample than for the concrete mixture. In other words, we consider that the powder samples contain the same proportions of sand and binder as in the concrete. The content of CaO obtained from the binder is then equal to α %CaO.

Knowing the CaO content in the binder used ($\%CaO_B$), it was then possible to deduce the binder content in the powder as:

$$\%B = \frac{\alpha\ \%CaO}{\%CaO_B} \quad (5)$$

1 $\%CaO_B$ was calculated from the CaO content of each binder (Table 1) and from the mix
2 proportions (Table 2) as follows:

$$\%CaO_B = \%CaO_{\text{CEM I, CEM II or CEM III}} \text{ for Ref I, Ref II or Ref III} \quad (6)$$

$$\%CaO_B = 0.70\ \%CaO_{\text{CEM I}} + 0.30\ \%CaO_{\text{FA or GGBFS}} \text{ for FA 30 or S 30} \quad (7)$$

$$\%CaO_B = 0.25\ \%CaO_{\text{CEM I}} + 0.75\ \%CaO_{\text{GGBFS}} \text{ for S 75} \quad (8)$$

3

4 where: $\%CaO_{\text{CEM I, CEM II or CEM III}}$ [%] are the CaO contents in CEM I, CEM II and CEM III,
5 respectively. $\%CaO_{\text{FA or GGBFS}}$ [%] are the CaO contents in FA and GGBFS, respectively.
6 For a given concrete, the binder contents of the powders taken between 0 and 45 mm, i.e., in
7 the specimen core, were close, whatever the exposure conditions. Similarly, the binder
8 contents of the powder samples taken at 55 mm, i.e., in the skin, were close. Fig. 4 shows the
9 effect of the location (core versus skin) on the binder contents. The average %B are different
10 from those calculated from the concrete composition given in Table 2 (relative difference
11 from 18 to 59 %). This was expected since powder sampling by drilling or planing does not
12 allow maintaining the initial composition. The binder content in the powders obtained by
13 removing the skin by planing is higher than that in the powders taken by drilling the core. The
14 observed relative difference of about 40 % is explained by the "skin-effect", which leads to a
15 surface layer richer in paste, thus in binder, than in the core (Kreijger, 1984). In the following,
16 the average binder contents shown in Fig. 4 were used to calculate the bound CO_2 content per
17 mass of binder. Different binder contents could have been used for each position. However,
18 we distinguished only two cases: samples in the core (between 0 and 45 mm from the center)
19 and samples in the skin (at 55 mm from the center). Let us recall that the sample is 110 mm
20 diameter. This procedure was preferred for less inaccuracy, since only one replicate was used
21 for chemical analysis.
22

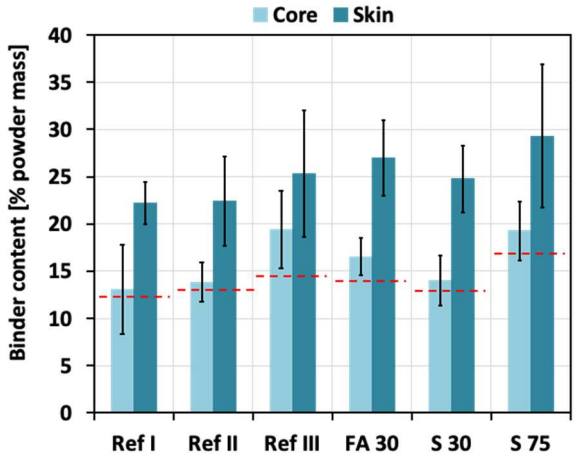

Fig. 4. Average binder contents in the powder samples determined by chemical analysis, in the specimen core (between 0 and 45 mm from the center) and in the skin (at 55 mm from the center). The red dashed lines give the theoretical binder contents from the concrete compositions (Table 2).

3.3. Profiles of bound CO_2 content per mass of binder

The bound CO_2 content at a location r, denoted $(\%CO_2)_r$, expressed by mass of binder was determined from TGA on powders as follows (Eq. 9):

$$(\%CO_2)_r = 100 \cdot \left(\frac{\Delta m_{T_1 \to T_2}}{\%B.\, m_P}\right)_r - 100 \cdot \beta \cdot \left(\frac{\Delta m_{T_1 \to T_2}}{\%B.\, m_P}\right)_{r=0} \quad (9)$$

where: $\Delta m_{T_1 \to T_2}$ [g] is the mass loss of the concrete powder during TGA in the temperature range [T_1-T_2]. Classically, T_1 and T_2 are close to 600°C and 900°C, respectively. %B [-] is the binder content in the powder assessed by ICP-AES (section 3.2). m_P [g] is the mass of the concrete powder tested by TGA. β is a correction factor accounting for the skin effect.

The center of the cylindrical specimen, i.e., r = 0, is unaffected by carbonation. The CO_2

content at this location results from the decarbonation of $CaCO_3$ supplied by both sand and binder. By subtracting the value at r = 0, we obtain only the CO_2 bound by carbonation. For r lower than 55 mm, the correction factor β is taken equal to 0. On the skin of the specimen, the $CaCO_3$ content before carbonation is not the same than at r = 0. The difference is due to higher contents of sand and binder (as shown in section 3.2). Thus, to determine the bound CO_2 content at r = 55 mm, the content of CO_2 at r = 0 in Equation 9 is corrected by β. The latter is calculated as the ratio of the binder content in the skin and the binder content in the core ($\beta > 1$). Note that we assume that the proportions sand/binder are the same in the skin than in the core.

Fig. 5 shows: (i) the carbonation fronts revealed by phenolphthalein spraying and (ii) the profiles of bound CO_2 content. The carbonation fronts are rather close to that suggested by the bound CO_2 content profiles determined by TGA/ICP-AES analysis. However, the latter shows that carbonation occurs more gradually, and in some cases more deeply than the pH front. This result is consistent with literature, e.g. (Omikrine-Metalssi et al., 2009).

In the area defined by the pH front, the profiles determined for the sheltered condition are up that for the unsheltered one. This suggests that unsheltered conditions, which strongly reduce the carbonation rate, also decrease the bound CO_2 content. The result, which corresponds to that of Houst and Wittmann (Houst et al., 2002), is not consistent with other studies which report that, due to high humidity, unsheltered conditions slightly increase the bound CO_2 content (Galan et al., 2010; Andrade et al., 2018). This result is discussed in section 4.1.

Ref III and S 75 exhibit maximum bound CO_2 contents that are about two times lower than that of the other concretes, despite their higher carbonation depths. Moreover, these two concretes bound more CO_2 in depth than in surface, although the binder content is higher in the specimen skin. This could be explained by the fact that these concretes, especially Ref III, are poorly hydrated in surface due to a too early demolding, as shown by numerical

computations in a previous study (Younsi et al., 2019). Anhydrous phases are less carbonatable than hydrates (Boumaaza et al., 2020b).

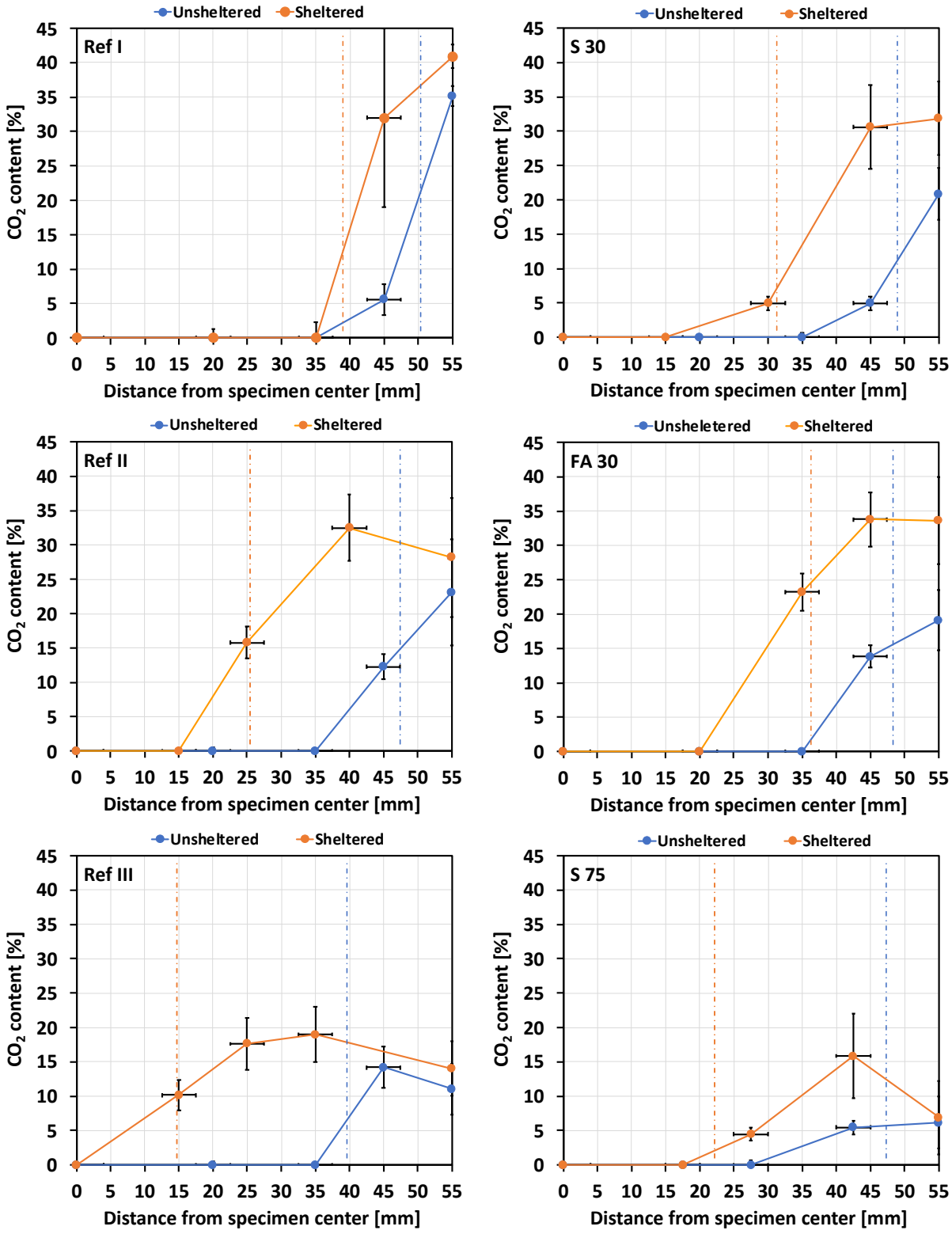

Fig. 5. Profiles of bound CO_2 content per mass of binder after 10-year natural carbonation. Dash lines and colored areas indicate the locations of carbonation fronts determined by means of phenolphthalein spraying and the variation ranges of these fronts, respectively (blue for unsheltered conditions and orange for sheltered).

3.4. CO_2 uptake

The CO_2 uptake was assessed from the profiles of bound CO_2 content following the steps. First, the content of bound CO_2 at a distance r from the core was expressed by volume of concrete [kg_{CO_2}/m^3]:

$$(CO_2)_r = B_r\ (\%CO_2)_r\ /\ 100 \tag{10}$$

where: $(\%CO_2)_r$ [%] is the bound CO_2 content at r expressed by mass of binder. B_r [kg_{binder}/m^3] is the binder content at r expressed by volume of concrete.

At the first 4 distances from the core, i.e., 0, (15 – 20), (20 – 35) and (35 – 45) mm, B_r was assumed to be equal to the binder content of the concrete mixture (Table 2). At 55 mm, B_r was calculated from this binder content multiplied by the ratio between the binder content determined in the skin and that determined at the other distances. This ratio, deduced from the profiles shown in Fig. 5, accounts for the fact that in the specimen skin, the binder content is higher due to the "skin-effect", which leads to a surface layer richer in binder (Kreijger, 1984). Moreover, as the skin was sampled to a depth of about 1 mm, both $(\%CO_2)_r$ and B_r were assumed to be constant between 54 and 55 mm. Examples of profiles of $(\%CO_2)_r$, B_r and $(CO_2)_r$ obtained for Ref I under sheltered conditions are given in Fig. 8.

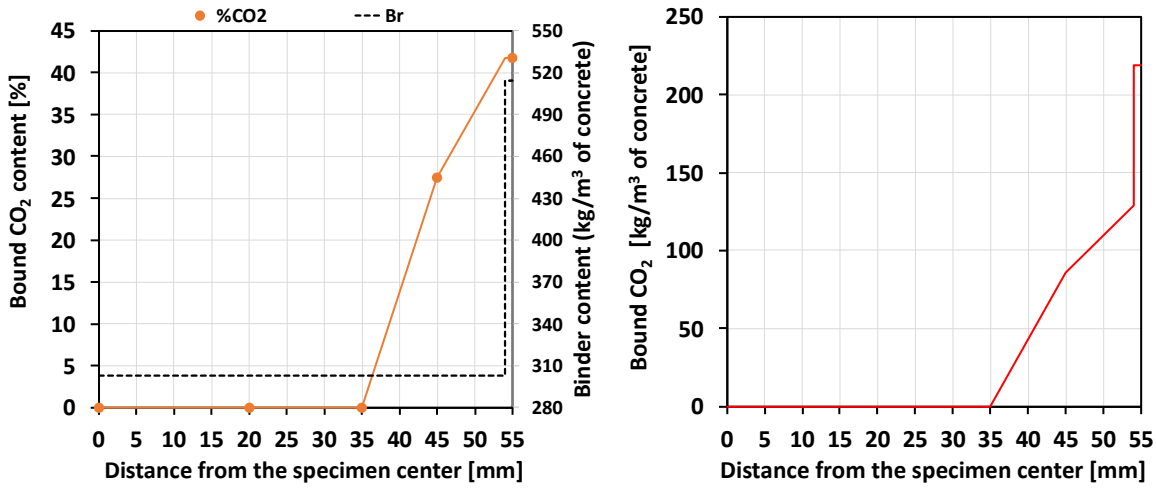

Fig. 6. Profiles of bound CO_2 content $(\%CO_2)_r$ expressed by mass of binder and binder content B_r expressed by volume of concrete (left), and profile of bound CO_2 content $(CO_2)_r$ expressed by volume of concrete (right): example of Ref I under sheltered conditions.

Second, the CO_2 binding capacity (CBC) of the carbonated zone revealed by phenolphthalein, expressed in kg_{CO_2}/m^3, was assessed by integration of the profile of $(CO_2)_r$:

$$CBC = \frac{2}{R^2} \int_{R-X_c}^{R} (CO_2)_r \, r dr \quad (11)$$

Table 4 gives the obtained value of CBC for each concrete. It should be noted that this value is an average CO_2 binding capacity of the carbonated zone, since the bound CO_2 is not necessarily uniform within this zone, as shown in Fig. 7. CBC as calculated is proposed because the depth X_c revealed by the pH indicator is usually the reference carbonation depth. It is also a comparison tool with the results of models such as that of standard EN 16757. Whatever the exposure condition, two sets of concretes can be distinguished: a set of

concretes with high CBC corresponding to concretes with binders of clinker content higher than 70%, i.e., Ref I, Ref II, FA 30 and S 30, and a set with lower CBC (up to two times lower), corresponding to concretes with clinker contents lower than 30%, i.e., Ref III and S 75.

In the third step, we determine the CO_2 uptake of the specimen expressed by exposure area by integrating the profile of $(CO_2)_r$:

$$\text{Uptake} = \frac{1}{R}\int_0^R (CO_2)_r \, r\,dr \tag{12}$$

Table 4 gives for each concrete the value of uptake, which quantifies the CO_2 bound by the cylindrical specimen after 10 years of exposure. The CO_2 uptake is at least 3 times higher in sheltered conditions than in unsheltered ones. For a given exposure, the differences in uptake between the studied concretes are rather low, especially for the unsheltered conditions.

Table 4

CO_2 binding capacity (CBC) of the carbonated zone revealed by phenolphthalein [kg_{CO_2}/m^3] and CO_2 uptake [kg_{CO_2}/m^2] determined from the profiles of bound CO_2 content.

	Sheltered conditions						Unsheltered conditions					
	Ref I	Ref II	Ref III	FA 30	S 30	S 75	Ref I	Ref II	Ref III	FA 30	S 30	S 75
CBC	107	81	57	115	79	47	103	70	42	79	57	41
Uptake	1.47	1.74	1.46	1.79	1.47	1.08	0.46	0.49	0.56	0.50	0.32	0.30

4. Discussion

4.1. Degree of carbonation

The degree of carbonation (DoC) is defined as the ratio between the bound CO_2 content ($\%CO_2$) and the theoretical maximum bound CO_2 content (U_B):

$$DoC = \frac{\%CO_2}{U_B} \quad (13)$$

U_B can be assessed using Equation (14) assuming that all calcium oxides of the binder are converted by carbonation into $CaCO_3$, except CaO reacting with SO_3 (Boumaaza et al., 2020b; Steinour, 1959):

$$U_B = \%CaO_B \cdot \frac{M_{CO_2}}{M_{CaO}} - \%SO_3 \cdot \frac{M_{CO_2}}{M_{SO_3}} \quad (14)$$

Where: M_{CO_2}, M_{CaO} and M_{SO_3} [g/mol] are the molar masses of CO_2, CaO and SO_3, respectively, $\%SO_3$ the SO_3 content in the binder [%] provided by binder producers and determined by XRF analysis (Table 1).

The highest degree of carbonation was calculated for each concrete and each exposure from the profile of bound CO_2 content (Figure 7-left). Note that the highest DoC are in the specimen skin, except for the mixtures with high content of GGBFS (Ref III and S 75). As shown in section 3.3, the latter tend to be more carbonated in depth than in surface, especially in unsheltered condition. Two parameters controlling DoC can be discussed: exposure and nature of binder.

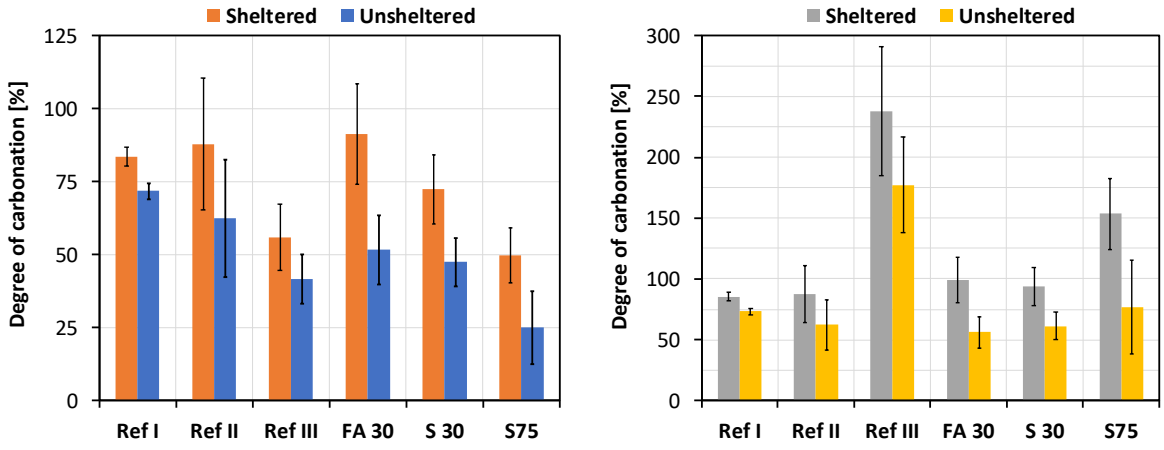

Fig. 7. The highest degrees of carbonation from the profiles of bound CO_2 content, calculated with the maximum bound CO_2 content considering carbonation of all CaO from binder (left) and with the maximum bound CO_2 content considering carbonation of CaO from the clinker only, as proposed by Standard EN1657 (right).

With respect to the effect of exposure conditions, DoC is found higher for sheltered specimens than for unsheltered ones. This result is a bit surprising since, in most of literature data, the degree of carbonation increases in the most wet conditions (Andrade, 2020; Andrade et al., 2018; Galan et al., 2010). This is usually explained by the fact that increasing the water saturation degree also increases the amount of available compounds for carbonation, since the carbonation reactions take place in the pore solution. As shown by (Boumaaza et al., 2020b; Steiner et al., 2020), ultimate DoC of hydrates depends strongly on the relative humidity. In our study, several reasons can be given to explain the lower degrees of carbonation in unsheltered conditions. First, it can be due to the sampling of powder at the specimen surface, especially in the case of Ref I, Ref II, FA 30 and S 30. The specimen skin not protected from rain was slightly degraded, probably due to leaching. It is therefore more difficult to have a precise determination of DoC at the specimen surface. It should be kept in mind that the carbonation depths determined for most of unsheltered specimens were low (around 5 mm)

and the profiles of bound CO_2 content rather sharp. Second, the oceanic climate of La Rochelle (France) is windy. Rapid and frequent drying due to sunshine and wind, followed by relatively short but heavy rainfall periods, could reduce the water content within the carbonated zone, which could slightly hamper the carbonation reactions. The water content however remains enough for slowing down the progress of the carbonation front. Under sheltered conditions, with an acceptable relative humidity of the environment, the concrete pore network remains partially saturated, perhaps even in equilibrium, which favors the carbonation reactions (Houst et al., 2002; Leeman et al., 2015; Ekolu, 2016). Third, the average temperatures of both exposure sites were not the same. The average temperature for the sheltered specimens was about 5°C higher and the temperature range narrower (Table 3). Although the influence of temperature on carbonation is difficult to understand because of contradictory effects on the involved mechanisms, it is recognized that carbonation rate increases when temperature increases, e.g., (Drouet et al., 2019). Finally, both exposure conditions used in the present study could lead to substantially equal degrees of carbonation. By way of comparison, note that Standard EN 16575 proposes close DoC values for the two types of exposure, i.e., 75% for sheltered condition and 80% for unsheltered one.

The nature of binder is also a parameter which has a huge effect on the degree of carbonation. It clearly appears that concretes with a high substitution of clinker by GGBFS, i.e., Ref III and S 75, have much lower DoC, as defined by Equation 13, despite their higher carbonation depths. There is no relationship between the carbonation depth, determined by means of a pH indicator, and the degree of carbonation (Omikrine-Metalssi et al., 2009; Andrade, 2020).

Ref III and S 75 exhibit the lowest average bound CO_2 contents although their CaO contents are close to those of FA 30 and Ref I, respectively (Table 2). To better understand this tendency, the degrees of carbonation were also calculated assuming that only calcium oxide from clinker can be carbonated. This approach is proposed by EN 16757, i.e., U_B is taken

equal to U_K. Fig. 8 shows the difference between U_K from EN 16757 and U_B calculated with the entire CaO content of the binder (Eq. 14). The highest differences are for mixtures with GGBFS. In the case of mixtures with fly ash, i.e., Ref II and FA 30, U_K and $\%CO_2 max$ are almost equal because of the very low CaO content of fly ash.

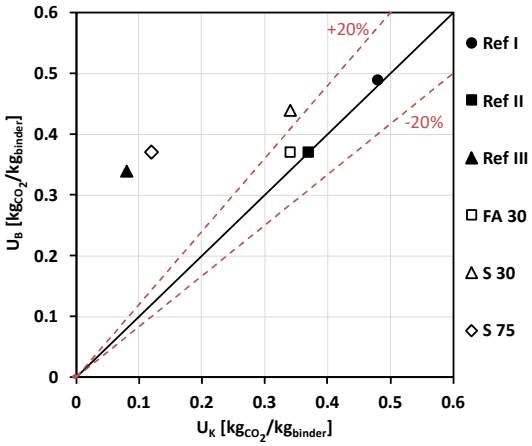

Fig. 8. Maximum theoretical bound CO_2 content as per the definition of this study (U_B) *versus* values obtained using EN 16757 (U_K).

In Figure 7 (right), the degrees of carbonation so obtained for the mixtures with GGBFS are much higher, and even higher than 100% (i.e., losing the physical sense of this parameter), as shown by Andrade (Andrade, 2020). This result highlights that a part of the calcium oxides supplied by GGBFS contributes to the uptake of CO_2. To assess the degree of carbonation of the calcium oxide from slag, the global DoC, as defined previously in Equation 13, was rewritten as follows:

$$DoC = 100\frac{\%CO_2}{U_B} = 100\frac{U_K \cdot DoC_K \cdot \%K + U_S \cdot DoC_S \cdot \%S}{U_B} \quad (15)$$

Where: U_i is the maximal content of CO_2 bound by CaO of the constituent i, DoC_i is the degree of carbonation of the constituent i, and %i is the content of i in the binder. K and S denote clinker and slag, respectively. U_i is calculated with the CaO content in the constituent i, (Equation 14).

In Equation 15, all parameters, except DoC_S, are known if we assume that DoC_K is equal to the degree of carbonation found for Ref I, i.e., the mixture made with a Portland cement. Calculated values of DoC_S are given in Table 5. These values are only rough estimations due to the high standard deviations obtained for DoC. These orders of magnitude show that the degree of carbonation of CaO from slag is much lower than that of CaO from clinker, but not negligible, except in unsheltered conditions. Our estimations confirm recent results of (Saillo et al, 2021) obtained from an in-depth study of the mineral changes in cement pastes due to carbonation. The authors show that calcium from slag is less carbonatable than that of clinker. Moreover, a large amount of slag can remain unreacted even after a long-term water curing. In our case, the specimens were removed from the mold after 1 day and exposed to drying, what strongly disadvantages hydration (Younsi et al., 2019). From our data, it remains however difficult to propose a single empirical value to predict the degree of carbonation of slag. Moreover, the combination of CO_2 with the cementitious elements is undoubtedly more complex than a simple separation of the binding capacity of CaO as a function of the constituent origin as proposed by Equation 15. The mineral assemblages of Portland cement and that of binders with GGBFS are quite different. GGBFS promotes calcium silicate hydrate (C-S-H) with lower Ca/Si ratio than that of Portland cement. Through experimental observations, (Steiner et al., 2020) confirms that the carbonation rate and the CO_2 binding capacity of C-S-H decreases with the Ca/Si ratio.

Table 5

Calculated degrees of carbonation: degree as defined in Eq. 15 (DoC), degree of CaO from Ref I binder (DoC_K) and degree of CaO from slag (DoC_S).

	Sheltered conditions			Unsheltered conditions		
	S 30	Ref III	S 75	S 30	Ref III	S 75
DoC (%)	72	56	50	47	42	25
DoC_K (%)	83	83	83	72	72	72
DoC_S (%)	31	48	32	~0	40	~0

4.2. CO_2 uptake

To analyze the CO_2 uptake of the studied specimens, the results obtained for mixture Ref I made with the high clinker content are used as reference values for comparison. The relative differences in CBC, X_c and CO_2 uptake are given in Figure 9. There is no clear correlation between the CO_2 binding capacity of the material and the CO_2 uptake of the specimen. For instance, Ref III has high relative differences in CBC (-50%) but CO_2 uptakes rather close to the uptake of Ref I (relative differences lower than 20%). In fact, as shown also in Figure 9, the relative differences in carbonation depth of Ref III are very high. For this concrete, the high carbonation depths partly compensate the lower binding capacity. A similar analysis can be made for Ref II, FA 30, S 30 and S 75.

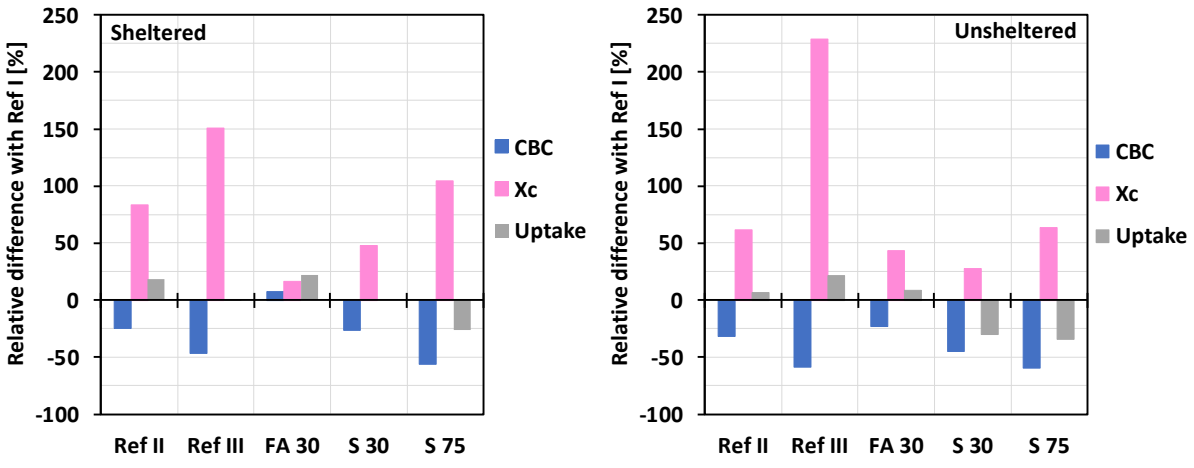

Fig. 9. Relative differences in CO_2 binding capacity (CBC), carbonation depth (X_c) and CO_2 uptake between Ref I and other studied concretes, for sheltered (left) and unsheltered (right) exposure conditions after 10 years of natural carbonation.

To highlight the effect of exposure, the results from experiments are presented differently in Figure 10. The latter gives the ratios of values for sheltered conditions and values for unsheltered ones. These ratios are between 1 and 1.8 for CO_2 binding capacity while they are much higher for carbonation depth and CO_2 uptake. This means that CBC is much less impacted by the exposure for all studied materials, than X_c and CO_2 uptake. Once again, the role of X_c is decisive for the CO_2 uptake at the specimen scale.

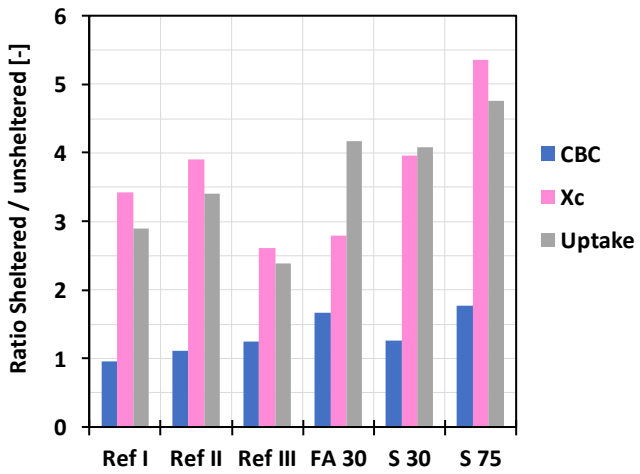

Fig. 10. Effect of exposure conditions on CO_2 binding capacity (CBC), carbonation depth (X_c) and CO_2 uptake: ratios of values for sheltered conditions and values for unsheltered ones.

4.3. Comparison with prediction of EN 16757 model

Figure 11 compares the CO_2 uptakes obtained experimentally and values calculated using the Standard EN 16757 model. The latter underestimates the uptake in sheltered conditions with

errors of at least 20% for most of concretes. The prediction is good only for Portland cement-based concrete, i.e., Ref I. The predictions are better for unsheltered concretes with errors lower than 20%, apart for Ref III whose predicted uptake is 3 times lower than that from experiments. To understand the differences between experimental and computed values, analysis can be made as previously, i.e., in terms of CBC and X_c.

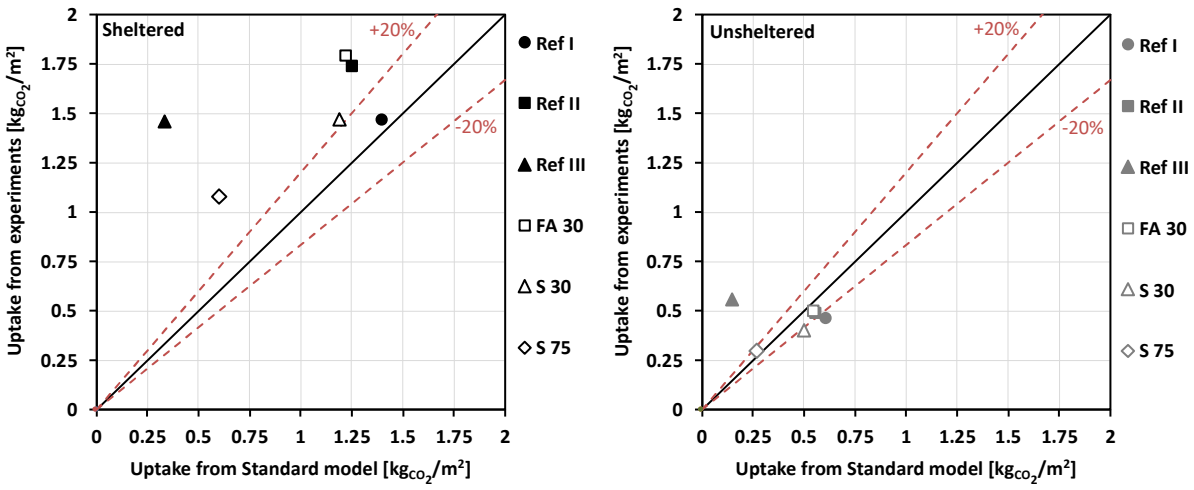

Fig. 11. CO_2 uptakes calculated from experimental data *versus* values calculated as per EN 16757: sheltered (left) and unsheltered conditions (right).

Figure 12 shows that the standard model tends to overestimate the binding capacities of concrete for unsheltered conditions, except for Ref III. The wrong estimation of CBC results from errors in degree of carbonation (DoC) and theoretical bound CO_2 content (U_B). In the case of concrete with high clinker content (Ref I, Ref II, FA 30 and S 30), the latter is correctly computed by the model, because U_B is equal to U_K (Fig. 8). Thus, the main error comes from DoC which is significantly lower from experiments than from the model (see section 4.1). In the case of Ref III, both DoC and U_B used by the model are not correct. Standard DoC (75 or 80%) is higher than experimental DoC (around 50%) and U_B is taken

equal to U_K considering that only calcium oxides from clinker can be carbonated, while, as shown previously, a part of CaO from slag also binds CO_2. However, the overestimation of DoC compensates partly the underestimation of U_B. Globally, the differences in CBC between experiments and model for Ref III are lower than the differences in CO_2 uptake.

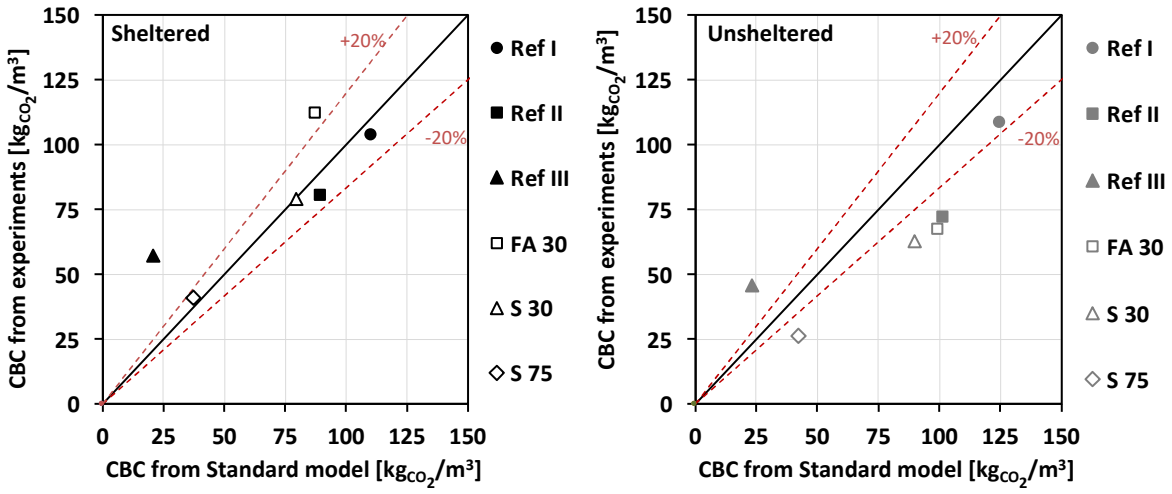

Fig. 12. CBC from experiments *versus* values calculated as per EN 16757: sheltered conditions (left) and unsheltered conditions (right).

As revealed by Figure 13, lot of the difference between experimental and computed values come from the underestimation of the carbonation depth by the model. Especially, for sheltered conditions, the model error is high for most of concretes. Prediction is good only for the Portland cement concrete. The model accuracy is better for the unsheltered conditions, apart for Ref III.

Finally, these analyses show that efforts to improve predictions of CO_2 uptake should focus primarily on the carbonation rate, which is not predicted with sufficient accuracy for concretes with low clinker content. As suggested by Andrade (Andrade, 2020), adjustments per country for the carbonation rate should be proposed because of the diversity of cements

used and exposure conditions. Another solution could be the extrapolation of the carbonation rate from results of accelerated carbonation tests, as proposed in models for service life design, e.g. (fib, 2006).

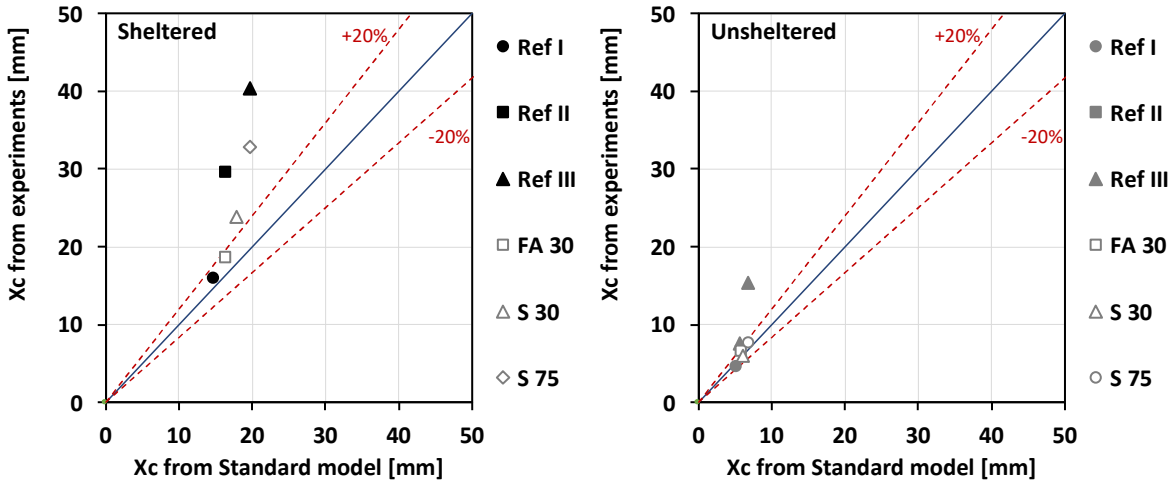

Fig. 13. Carbonation depths from experiments *versus* values as per EN 16757: sheltered conditions (left) and unsheltered conditions (right).

5. Conclusions

An experimental study of CO_2 uptake after 10 years natural carbonation was carried out on concretes designed with Portland cement (OPC), blended cements containing fly ash (FA) or ground granulated bast furnace slag (GGBFS) and partial substitutions of OPC with FA (30 %) or GGBFS (30 and 75 %). These concretes were designed to have equivalent strengths at early age and 28 days. 1 day after casting, concrete cylinders were subjected to a 10-year natural carbonation, under sheltered and unsheltered conditions. The CO_2 uptake, i.e., the bound CO_2 content per m^2 of exposed surface, was determined from profiles of bound CO_2 obtained by TGA and chemical analyses. The main conclusions are the following.

- 10-year natural carbonation monitoring shows that the concretes with cement substitution with fly ash or GGBFS have carbonation depths close to those of concretes with blended cements containing the same additions. Thus, their potential durability is at least equivalent to that of the latter. This confirms prediction from previous studies based on accelerated carbonation tests.
- The concretes kept in sheltered conditions have higher CO_2 uptake than in unsheltered conditions. In sheltered conditions, the CO_2 uptake was between 1.1 and 1.8 kg/m² (of exposure area) while in unsheltered ones it was between 0.3 and 0.6 kg/m², depending on the concrete mixture. This is mainly due to the deeper ingress of CO_2 when concrete is sheltered from rain and remains under more stable moisture conditions.
- The CO_2 binding capacity, i.e., the bound CO_2 content in the carbonated depth, was found lower in the rainy conditions than in the sheltered one, what was somewhat unexpected with respect to literature. This tendency could be due to differences in parameters such as temperature or drying rate between both exposure conditions. The following conclusions are the same whatever the exposure conditions.
- CO_2 binding for concretes with high content of GGBFS consumes calcium oxides from both clinker and GGBFS. However, the degree of carbonation of CaO from GGBFS is much lower than the degree of carbonation of CaO from clinker. The low Ca/Si ratio of C-S-H produced by hydration of GGBFS and poor hydration degree of GGBFS could explain this finding. As a result, the CO_2 binding capacity is up to two times lower for the concretes with high content of GGBFS than for the other studied concretes.
- No correlation was found between the CO_2 binding capacity of the material and the CO_2 uptake of the specimen. Concretes with the lowest CO_2 binding capacity have also the highest carbonation depth. Since the CO_2 uptake can be assessed as the product of the CO_2 binding capacity and the carbonation depth determined from pH change (accounting for

the structure geometry), a low CO_2 binding capacity can be partly compensated by a high carbonation depth.

- The model from the Annex BB of the European Standard EN 16757 underestimates the CO_2 uptakes, especially for concretes under sheltered conditions and concretes with high content of GGBFS. The predictions were found correct mainly for the OPC concrete. The wrong estimation of the CO_2 uptake comes from wrong estimation of the CO_2 binding capacity but, above all, from misestimation of the carbonation depth.

Based on these results, some adjustments of the European Standard EN 16757 could be proposed to better assess the CO_2 uptake, especially for concretes with high GGBFS content. In terms of carbonation rate, the adjustment factors defined by the standard to account for the effect of mineral additions should be increased. In the design phase of a project, the carbonation rate could be deduced from accelerated carbonation test, rather than assessed from tabulated values. In terms of CO_2 binding capacity of concrete with high GGBFS content, two approaches could be suggested. First, the CO_2 binding capacity can be calculated considering only CaO from clinker and high degree of carbonation, as proposed in the present model. This approach leads to an underestimation of the binding capacity, which could be viewed as a "safety approach". Second, the CO_2 binding capacity could be calculated more realistically considering all the CaO from the binder, but with degree of carbonation at least two times lower than that proposed currently. Further in-deep research is needed to better define the degree of natural carbonation of hydrates produced by GGBFS.

Also, for a better representativeness, this study should be extended to concretes from old real structures but including different types of binders.

CRediT authorship contribution statement

Akli Younsi: Conceptualization, Methodology, Validation, Investigation, Resources, Writing - Original Draft, Writing - Review & Editing, Visualization, Supervision. **Philippe Turcry:** Conceptualization, Methodology, Validation, Investigation, Resources, Writing - Review & Editing, Visualization. **Abdelkarim Aït-Mokhtar:** Validation, Resources, Writing - Review & Editing, Visualization.

Declaration of Competing Interest

The authors declare that they have no known competing financial interests or personal relationships that could have appeared to influence the work reported in this paper.

Acknowledgments

The authors would like to acknowledge the French National Federation of Public Works (FNTP) for funding the carbonation characterization by TGA/ICP-AES, the French National Research Agency (ANR) for funding the *EcoBéton* project during which the concrete mixtures studied were designed, and Carine Churlaud (La Rochelle University, LIENSs UMR CNRS 7266) for the chemical analyzes ICP-AES. The authors would like also to acknowledge Emmanuel Rozière (GeM, UMR CNRS 6183, Ecole Centrale Nantes) for supplying a sample of sand.

Appendix – Calculation of the time-evolution of the carbonation depth in cylindrical geometry

First, let us recall how we obtain the time-evolution of the carbonation depth in axial geometry (i.e., the "classic" square-root of time model).

Several assumptions were made:

- The main parameters, i.e., the gaseous CO_2 diffusion coefficient (D), the content of carbonatable compounds in concrete (n_c) and the ambient concentration of CO_2 (C_0), were assumed to be constant.
- The chemical reactions were assumed to be much faster than the gas diffusion. As a result, the carbonation front progresses only when all the carbonatable compounds at the front are consumed. The front separates two zones, a "completely" carbonated zone where CO_2 diffuses and, more in depth, a non-carbonated zone where the concentration of CO_2 is null.

In the carbonated zone, the Fick's second law can be applied:

$$\frac{\partial C}{\partial t} = D\frac{\partial^2 C}{\partial x^2} \quad \text{(A.1)}$$

Where: C is the concentration of gaseous CO_2 at time t and depth x.

Due to the second assumption, the time variation of the concentration of CO_2 is very small ($\partial C/\partial t \approx 0$). Thus, the profile of C is a linear function of the depth x:

$$C = C_0\left(1 - \frac{x}{x_c}\right) \quad \text{(A.2)}$$

Where: x_c is the carbonation depth.

At the carbonation front, the amount of CO_2 diffusing through a surface S during a time dt is consumed by the carbonatable compounds in an elementary volume $dV = Sdx_c$:

$$-SD\frac{\partial C}{\partial x}dt = n_c dV \qquad \Leftrightarrow \qquad D\frac{C_0}{n_c}dt = x_c dx_c \tag{A.3}$$

By integrating Equation (A.3), the time evolution of the carbonation depth can be written as:

$$X_c = \sqrt{\frac{2DC_0}{n_c}}\sqrt{t} \tag{A.4}$$

In the case of a cylindrical geometry with a radial diffusion, the previous model cannot be applied because the Fick's second law takes a different form:

$$\frac{\partial C}{\partial t} = D\frac{\partial^2 C}{\partial r^2} + \frac{D}{r}\frac{\partial C}{\partial r} \tag{A.5}$$

Where r is the radial location, so as r = R – x, with R is the radius of the cylinder.

With the same assumption than previously (very small time-variations), the profile of CO_2 concentration as a function of x can be written as a function of the depth x:

$$C = C_0\left(\frac{\ln(R-x) - \ln(R-x_c)}{\ln(R) - \ln(R-x_c)}\right) \tag{A.6}$$

Then, from the equality of the diffusing and the consumed amounts of CO_2:

$$-SD\frac{\partial C}{\partial x}dt = n_c dV \qquad \Leftrightarrow \qquad D\frac{C_0}{n_c}dt = (R-x_c)\big(\ln(R) - \ln(R-x_c)\big)dx_c \tag{A.7}$$

By integrating Equation (A.7), we establish the following relationship between carbonation depth and time:

$$D\frac{C_0}{n_c}t = -\frac{X_c^2}{4} - \ln(R)\frac{X_c^2}{2} + \ln(R - X_c)\frac{(R - X_c)^2}{2} + R\ln(R)X_c + R\frac{X_c}{2} + \frac{R^2\ln(R)}{4} \quad (A.8)$$

Equation (A.8) can be solved numerically to determine X_c at a given time t. The left-hand side parameter DC_0/n_c can be deduced from empirical models giving X_c as a function of the square-root of time (axial geometry), such as the model from standard EN16575:

$$X_c = A\sqrt{t} \quad (A.9)$$

From Equation (A.4), DC_0/n_c is thus equal to $A^2/2$.

Figure A.1 compares results obtained for both geometries, i.e., axial and cylindrical: carbonation depths (related to the cylinder radius R) as a function of time from Equation A.4 and A.8, respectively. These results were obtained for a cylinder of 55 mm in radius, a CO_2 concentration of 500 ppm (2.10^{-2} mol/m^3), a diffusion coefficient of 5.10^{-7} m^2/s and a concentration of carbonatable compounds of 1000 mol/m^3. The difference between values from both geometries remains small when the carbonation depth X_c is lower than 40% of the specimen radius, i.e., 22 mm for the present example. Beyond this ratio, the use of Equation A.6 is necessary to calculate the time-evolution of X_c for a radial carbonation, instead of the classical square-root of time model (with the same assumption than the latter, e.g., a constant DC_0/n_c).

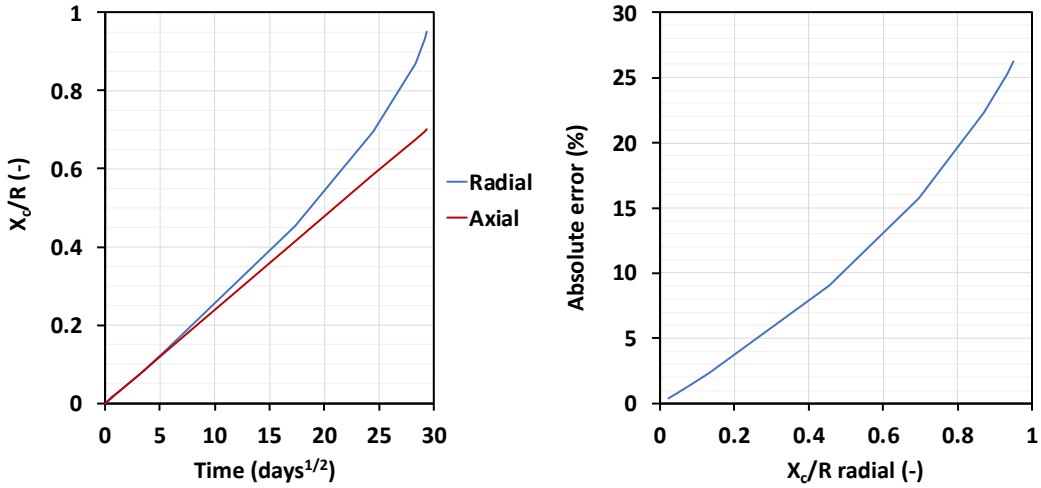

Fig. A.1. Comparison of calculated values for axial and cylindrical geometries: ratio between carbonation depth and radius versus square root of time (left) and absolute error versus the ratio for the cylindrical geometry (right). Calculations were done using data given in the text.

References

Andersson, R., Fridh, K., Stripple, H., Häglund, M., 2013. Calculating CO_2 uptake for existing concrete structures during and after service life. Environ. Sci. Technol. 47, 11625–11633. https://doi.org/10.1021/es401775w.

Andersson, R., Stripple, H., Gustafsson, T., Ljungkrantz, C., 2019. Carbonation as a method to improve climate performance for cement-based material. Cem. Concr. Res. 124, 105819. https://doi.org/10.1016/j.cemconres.2019.105819.

Andrade, C., Sanjuán, M., 2018. Updating Carbon Storage Capacity of Spanish Cements. Sustainability 10. https://doi.org/10.3390/su10124806.

Andrade, C., 2020. Evaluation of the degree of carbonation of concretes in three environments. Constr. Build. Mater. 230. https://doi-org.gutenberg.univ-lr.fr/10.1016/j.conbuildmat.2019.116804.

Andrew, R.M., 2019. Global CO2 emissions from cement production, 1928–2018. Earth Syst. Sci. Data. 11, 1675–1710. https://doi.org/10.5194/essd-11-1675-2019.

Ashraf, W., 2016. Carbonation of cement-based materials: challenges and opportunities. Constr. Build. Mater. 120, 558–570. https://doi.org/10.1016/j.conbuildmat.2016.05.080.

Bordy, A., Younsi, A., Aggoun, S., Fiorio, B., 2017. Cement substitution by a recycled cement paste fine: role of the residual anhydrous clinker. Constr. Build. Mater. 132, 1–8. https://doi.org/10.1016/j.conbuildmat.2016.11.080.

Boumaaza, M., Turcry, Ph., Huet, B., Aït-Mokhtar, A., 2020. Influence of carbonation on the microstructure and the gas diffusivity of hardened cement pastes. Constr. Build. Mater. 253, 119-227. https://doi.org/10.1016/j.conbuildmat.2020.119227.

Boumaaza, M., Huet, B., Turcry, Ph., Aït-Mokhtar, A., 2020. The CO_2-binding capacity of synthetic anhydrous and hydrates: Validation of a test method based on the instantaneous reaction rate. Cem. Concr. Res. 135. https://doi.org/10.1016/j.cemconres.2020.106113.

Costa, F.N., Ribeiro, D.V., 2020. Reduction in CO_2 emissions during production of cement, with partial replacement of traditional raw materials by civil construction waste (CCW). J. Clean. Prod. 276, 123302. https://doi.org/10.1016/j.jclepro.2020.123302.

Drouet, E., Poyet, S., Le Bescop, P., Torrenti, J.M., Bourbon, X., 2019. Carbonation of hardened cement pastes: influence of temperature. Cem. Concr. Res., 115, 445-459.

Ekolu, S.O., 2016. A review on effects of curing, sheltering, and CO_2 concentration upon natural carbonation of concrete. Constr. Build. Mater. 127, 306–320.

Elchalakani, M., Basarir, H., Karrech, A., 2017. Green concrete with high-volume fly ash and slag with recycled aggregate and recycled water to build future sustainable cities. J. Mater. Civ. Eng. 29. https://doi.org/10.1061/(asce)mt.1943-5533.0001748.

Esfahani, S.M.R.A., Zareei, S.A., Madhkhan, M., Ameri, F., Rashidiani, J., Taheri, R.A., 2021. Mechanical and gamma-ray shielding properties and environmental benefits of concrete incorporating GGBFS and copper slag. J. Build. Eng. 33, 101615. https://doi.org/10.1016/j.jobe.2020.101615.

Feiz, R., Ammenberg, J., Baas, L., Eklund, M., Helgstrand, A., Marshall R., 2015. Improving the CO_2 performance of cement, part I: utilizing life-cycle assessment and key performance indicators to assess development within the cement industry. J. Clean. Prod. 98, 272–281. http://dx.doi.org/10.1016/j.jclepro.2014.01.083.

Fitzpatrick, D., Richardson, M., Nolan, E., 2015. Sequestration of carbon dioxide by concrete infrastructure: a preliminary investigation in Ireland. J. Sustain. Archit. Civ. Eng. 1, 66–77. https://doi.org/10.5755/j01.sace.10.1.8037.

Flower, D.J.M., Sanjayan, J.G., 2007. Greenhouse gas emissions due to concrete manufacture. Int. J. Life Cycle Assess. 12, 282–288. http://dx.doi.org/10.1007/s11367-007-0327-3.

Galan, I., Andrade, C., Mora, P., Sanjuan, M.A., 2010. Sequestration of CO_2 by concrete carbonation. Environ. Sci. Technol. 44, 3181–3186. https://doi.org/10.1021/es903581d.

Gartner, E., Hirao, H., 2015. A review of alternative approaches to the reduction of CO_2 emissions associated with the manufacture of the binder phase in concrete. Cem. Concr. Res. 78, 126–142. http://dx.doi.org/10.1016/j.cemconres.2015.04.012.

Houst, Y.F., Wittmann, F.H., 2002. Depth profiles of carbonates formed during natural carbonation. Cem. Concr. Res. 32, 1923–1930.

Huy Vu, Q., Pham, G., Chonier, A., Brouard, E., Rathnarajan, S., Pillai, R., Gettu, R., Santhanam, M., Aguayo, F., Folliard, K.J., Thomas, M.D., Moffat, T., Shi, C., Sarnot, A., 2019. Impact of different climates on the resistance of concrete to natural carbonation. Constr. Build. Mater. 216, 450–467. https://doi.org/10.1016/j.conbuildmat.2019.04.263.

Jang, J.G., Kim, G.M., Kim, H.J., Lee, H.K., 2016. Review on recent advances in CO_2 utilization and sequestration technologies in cement-based materials. Constr. Build. Mater. 127, 762–773. https://doi-org.gutenberg.univ-lr.fr/10.1016/j.conbuildmat.2016.10.017.

Kangni-Foli, E., Poyet, S., Le Bescop, P., Charpentier, T., Bernachy-Barbe, F., Dauzeres, A., L'Hopital, E., d'Espinose de Lacaillerie, J.-B., 2021. Carbonation of model cement pastes:

The mineralogical origin of microstructural changes and shrinkage. Cem. Concr. Res. 144, 106446. https://doi.org/10.1016/j.cemconres.2021.106446.

Khokhar, M.I., Roziere, E., Turcry, Ph., Grondin, F., Loukili, A., 2010. Mix design of concrete with high content of mineral additions: optimisation to improve early age strength. Cem. Concr. Compos. 32, 377–385. http://dx.doi.org/10.1016/j.cemconcomp.2010.01.006.

Kreijger, P.C., 1984. The skin of concrete composition and properties. Mat. Constr. 17, 275–283. https://doi.org/10.1007/BF02479083.

Kwon, S.-J., Wang, X.-Y., 2021. CO_2 uptake model of limestone-powder-blended concrete due to carbonation. J. Build. Eng. 38, 102176. https://doi.org/10.1016/j.jobe.2021.102176.

Lagerblad, B., 2005. Carbon dioxide uptake during concrete life cycle – State of the art. Swedish Cem. Concr. Res. Inst.

Lee, H., Wang, X., 2016. Evaluation of the carbon dioxide uptake of slag-blended concrete structures, considering the effect of carbonation. Sustainability. 8, 312–329. https://doi.org/10.3390/su8040312.

Leemann, A., Nygaard, P., Kaufmann, J., Loser, R., 2015. Relation between carbonation resistance, mix design and exposure of mortar and concrete. Cem. Concr. Compos. 62, 33–43. https://doi.org/10.1016/j.cemconcomp.2015.04.020.

Lim, T.H., Ellis, B.L., Skerlos, S.J., 2019. Mitigating CO_2 emissions of concrete manufacturing through CO_2-enabled binder reduction. Environ. Res. Lett. 14, 114014. https://doi.org/10.1088/1748-9326/ab466e

Miller, S.A., Horvath, A., Monteiro, P.J.M., 2016. Readily implementable techniques can cut annual CO2 emissions from the production of concrete by over 20%. Environ. Res. Lett. 11, 074029. https://doi.org/10.1088/1748-9326/11/7/074029

fib, 2006. Model Code for Service Life Design, Bulletin No. 34.

Olivier, J.G.J., Janssens-Maenhout, G., Muntean, M., Peters, J.A.H.W., 2016. Trends in global

CO_2 emissions: 2016 report, PBL Netherlands Environmental Assessment Agency, European Commission, Joint Research Centre, https://www.pbl.nl/en/publications/trends-in-global-CO2-emissions-2016-report.

Omikrine-Metalssi, O., Aït-Mokhtar, A., 2009. A proposed methodology for a quantitative investigation of carbonation in polymer-modified mortars. Experimental Techniques, 33, 59-65.

Otieno, M., Ikotun, J., Ballim, Y., 2020. Experimental investigations on the effect of concrete quality, exposure conditions and duration of initial moist curing on carbonation rate in concretes exposed to urban, inland environment. Constr. Build. Mater. 246, 118443.

Pade, C., Guimaraes, M., 2007. The CO_2 uptake of concrete in a 100-year perspective. Cem. Concr. Res. 37, 1348–1356. https://doi.org/10.1016/j.cemconres.2007.06.009.

Papadakis, V.G., Vayenas, C.G., Fardis, M.N., 1991. Fundamental modeling and experimental investigation of concrete carbonation. ACI Materials Journal 88, 363-373.

Possan, E., Felix, E., Thomaz, W., 2016. CO_2 uptake by carbonation of concrete during life cycle of building structures. J. Build. Rehabil. 1 -7. https://doi.org/10.1007/s41024-016-0010-9.

Ren, C., Wang, W., Yao, Y., Wu, S., Qamar, Yao, X., 2020. Complementary use of industrial solid wastes to produce green materials and their role in CO_2 reduction. J. Clean. Prod. 252, 119840. https://doi.org/10.1016/j.jclepro.2019.119840.

Saillio, M, Baroghel-Bouny, V, Pradelle, S., Bertin, M., Vincent, J., d'Espinose de Lacaillerie, J.B. Effect of supplementary cementitious materials on carbonation of cement pastes. Cem. Concr. Res. 142 (2021) 106358

Sanjuán, M., Estevez, E., Argiz, C., 2019. Carbon dioxide absorption by blast-furnace slag mortars in function of the curing intensity. Energies 2346. https://doi.org/10.3390/en12122346.

Sanjuán, M.A., Andrade, C., Mora, P., Zarogoza A., 2020. Carbon dioxide uptake by cement-based materials: A Spanish case study. Appl. Sci. 10, 339. https://doi.org/10.3390/app10010339.

EN 16757 Standard, 2017. Sustainability of construction works – Environmental product declaration – Product Category Rules for concrete and concrete elements.

EN 197-1 Standard, 2011. Cement – Part 01:00 Composition, specifications and conformity criteria for common cements.

EN 450-1 Standard 2012. Fly ash for concrete – Part 01:00 Definition, specifications and conformity criteria.

EN 15167-1 Standard, 2006. Ground granulated blast furnace slag for use in concrete, mortar and grout – Part 01:00 Definitions, specifications and conformity criteria.

EN 13139 Standard, 2003. Aggregates for mortar.

EN 934-2+A1 Standard, 2012. Admixtures for concrete, mortar and grout – Part 02:00 Concrete admixtures – Definitions, requirements, conformity, marking and labelling.

EN 206/CN Standard, 2014. Concrete, specification, performance, production and conformity.

EN 12390-12 Standard, 2020. Testing hardened concrete – Part 12:00 Determination of the carbonation resistance of concrete – Accelerated carbonation method.

Steiner, S., Lothenbach, B., Proske, T., Borgschulte, A., Winnefeld, F., 2020. Effect of relative humidity on the carbonation rate of portlandite, calcium silicate hydrates and ettringite. Cem. Concr. Res. 135. https://doi.org/10.1016/j.cemconres.2020.106116.

Steinour, H.H., 1959. Some effects of carbon dioxide on mortars and concrete discussion. J. Am. Concr. Inst. 30, 905–907.

Thiery, M., Villain, G., Dangla, P., Platret, G., 2007. Investigation of the carbonation front shape on cementitious materials: effects of the chemical kinetics. Cem. Concr. Res. 37, 1047–1058. https://doi.org/10.1016/j.cemconres.2007.04.002.

Thiery, M., 2005. Modélisation de la carbonatation atmosphérique des matériaux cimentaires. Prise en compte des effets cinétiques et des modifications microstructurelles et hydriques, Ph.D. Thesis, LCPC Paris (in French).

Turcry, Ph., Oskri-Nelfia, L., Younsi, A., Aït-Mokhtar, A., 2014. Analysis of an accelerated carbonation test with severe preconditioning. Cem. Concr. Res. 57, 70–78. https://doi.org/10.1016/j.cemconres.2014.01.003.

Villain, G., Thiery, M., Platret, G., 2007. Measurement methods of carbonation profiles in concrete: thermogravimetry, chemical analysis and gammadensimetry. Cem. Concr. Res. 37, 1182–1192. https://doi.org/10.1016/j.cemconres.2007.04.015.

Witkowski, H., Koniorczyk, M., 2020. The influence of pozzolanic additives on the carbonation rate and Life Cycle Inventory of concrete. Constr. Build. Mater. 254, 119301. https://doi.org/10.1016/j.conbuildmat.2020.119301.

Xi, F., Davis, S.J., Ciais, P., Crawford-Brown, D., Guan, D., Pade, C., Shi, T., Syddall, M., Lv, J., Ji, L., Bing, L., Wang, J., Wei, W., Yang, K.-H., Lagerblad, B., Galan, I., Andrade, C., Zhang, Y., Liu, Z., 2016. Substantial global carbon uptake by cement carbonation. Nat. Geosci. 9, 880–883. https://doi.org/10.1038/ngeo2840.

Yang, K.-H., Seo, E.-A., Tae, S.-H., 2014. Carbonation and CO_2 uptake of concrete. Environ. Impact Assess. Rev. 46, 43–52. https://doi.org/10.1016/j.eiar.2014.01.004.

Yoon, I.-S., Çopuroglu, O., Park, K.-B., 2007. Effect of global climatic change on carbonation progress of concrete. Atmos. Environ. 41, 7274–7285. https://doi.org/10.1016/j.atmosenv.2007.05.028.

Younsi, A., Turcry, Ph., Rozière, E., Aït-Mokhtar, A., Loukili, A., 2011. Performance-based design and carbonation of concrete with high fly ash content. Cem. Concr. Compos. 33, 993–1000. http://dx.doi.org/10.1016/j.cemconcomp.2011.07.005.

Younsi, A., Turcry, Ph., Aït-Mokhtar, A., Staquet, S., 2013. Accelerated carbonation of

concrete with high content of mineral additions: effect of interactions between hydration and drying. Cem. Concr. Res. 43, 25–33. https://doi.org/10.1016/j.cemconres.2012.10.008.

Younsi, A., Turcry, Ph., Aït-Mokhtar, A., Staquet, S., 2019. Numerical study of the influence of drying on properties governing the carbonation mechanism of concretes with low clinker content. Eur. J. Environ. Civ. Eng. 23, 172–192. https://doi.org/10.1080/19648189.2016.1271364.

Younsi, A., Cherif, R., Trabelsi, A., Hamami, A.E.A., Belarbi, R., Aït-Mokhtar, A., 2021. Hydration-drying interactions in a high-volume ground granulated blast-furnace slag mortar. Constr. Build. Mater. 279, 122427. https://doi.org/10.1016/j.conbuildmat.2021.122427.

Younsi, A., Bordy, A., Aggoun, S., Fiorio, B., 2018. Hydration-drying interactions in OPC pastes blended with recycled OPC paste fine powder: critical curing relative humidity hampering hydration. Constr. Build. Mater. 90, 403–413. https://doi.org/10.1016/j.conbuildmat.2018.09.132